The optical variability of QSOs

II. The wavelength dependence[*],[**]

S. Cristiani[1], S. Trentini[1], F. La Franca[2], and P. Andreani[1]

[1] Dipartimento di Astronomia, Università di Padova, Vicolo dell'Osservatorio 5, I-35122 Padova, Italy

[2] Dipartimento di Fisica, Università degli Studi "Roma Tre", Via della Vasca Navale 84, I-00146 Roma, Italy

Abstract. The long-term variability of a sample of 149 optically selected QSOs in the field of the Selected Area 94 has been studied in the R-band. The relations between variability and luminosity and between variability and redshift have been investigated by means of "robust" statistical estimators, allowing to disentangle the effects of the measurement errors. The results are compared with the corresponding properties of the variability in the B-band for the same sample. An anti-correlation between the R-band variability and the intrinsic luminosity is found, analogously to what is observed in the B-band. The amplitude of the R-band variability turns out to be smaller (of a factor 1.13 ± 0.05) than the B-band variability. The implications in terms of the black-hole, starburst and microlensing models are discussed.

Key words: quasars: general

1. Introduction

The detailed study of statistically well-defined samples of optically selected QSOs is beginning to pin down their ensemble variability properties. An anti-correlation between variability and luminosity has been observed, such that more luminous QSOs show a smaller amplitude of the variations (Hook 1994, Cristiani et al. 1996). It starts also to emerge from the statistical noise a positive correlation between the amplitude of the variability and the redshift (Giallongo et al. 1991, Trevese et al. 1994, Cristiani et al. 1996, Cid Fernandes et al. 1996). This latter dependence may be interpreted as an anti-correlation between amplitude of the variability and wavelength in the individual objects (Cristiani et al. 1996, Cid Fernandes et al. 1996, Di Clemente et al. 1996),

as suggested by observations of relatively small samples of objects (Perola et al. 1982, Edelson et al. 1990, Kinney et al. 1991, Paltani & Courvoisier 1994). Both properties bear important implications for the understanding of the AGN energy generation mechanism and distinguishing among the competing variability models based on the black-hole (Rees 1984), starburst (Terlevich et al. 1992) and microlensing (Hawkins 1993, 1996) scenarios. At the same time they are central for the quantification of the biases affecting samples selected on the sole basis of variability (Véron & Hawkins 1995) or on the basis of multicolor data, if the photometry was carried out at different epochs in the various wavebands (e.g. Warren et al. 1991).

However the variability-redshift correlation could be due to an evolutionary effect, in the sense of a higher activity in the early phases of the AGN life. The only way to remove such an uncertainty is to check directly the variability properties of individual objects, by observing them simultaneously in two or more wavebands. For this reason we have investigated the R-band variability of the SA94 QSO sample, the same that in Cristiani et al. 1996 (in the following Paper I) had been studied in the B band.

We report in Sect. 2 the description of the SA94 QSO sample and the photometric material used to investigate its variability; in Sect. 3 the ensemble structure function is introduced as a statistical measure of the variability properties and the detected trends are further analysed with the aid of other statistical indices; the results and implications are discussed in Sect. 4.

Throughout the paper we have assumed cosmological constants $H_o = 50$ km sec^{-1} Mpc^{-1} , $q_o = 0.5$.

2. The quasars sample

2.1. Definition of the sample

The SA94 sample is made up of 149 optically selected quasars [1] listed in Table 1, observed in a rectangular area of the sky within

---

---

[1] In the present paper quasars are defined as objects with a starlike nucleus, broad emission lines, brighter than $M_B = -23$ mag, applying the K-corrections computed on the basis of the composite spectrum

Table 2. List of the plates

Plate	Exp (min)	Date	Epoch/date	Limit (mag)
E1453	40-60	1955 Oct 22	1 (1955.81)	19.5
R5413	60	1983 Dec 08	2 (1983.94)	20.3
R5414	60	1983 Dec 08	2 (1983.94)	20.3
R12218	150	1987 Oct 16	3 (1987.79)	20.1
R12807	140	1988 Oct 15	4 (1988.79)	19.5
R13409	100	1989 Oct 28	5 (1989.83)	20.1
R13420	100	1989 Nov 01	5 (1989.83)	20.1
R8757	120	1990 Sep 21	6 (1990.72)	19.1
R9477	120	1991 Oct 07	7 (1991.77)	17.3

the limits $2^h43^m51.2^s < \alpha < 2^h59^m14.3^s$, $-2°03'23.8'' < \delta < 2°32'11.0''$ (Epoch 1950.0), covering 17.66 sq. deg.

They have been mainly discovered in the UVx and objective-prism surveys described in Paper I and in the references to Table 1.

### 2.2. Calibration of the photographic material and error estimation

8 plates taken with the ESO La Silla and UK Schmidt telescopes and a copy of a POSS E-plate (E1453) have been analysed. In Table 2 a detailed list is given. The combination IIIa-F + RG630 filter was used in all cases except for the plate E1453, that is a combination of a IIIa-E + a red Plexiglas 2444, providing a transmission similar to that of a Wratten $n°29$ filter (peak sensitivity near $\lambda6563$). The natural photometric system defined by the IIIa-F + RG630 combination (in the following defined R') is close to the Johnson-Kron-Cousins R and the color transformation is given by Bessel (1986):

$$R' = R - 0.013 - 0.201\,(R - I) + 0.100\,(R - I)^2 + \\ +0.0295\,(R - I)^3 \qquad (1)$$

The combination IIIa-E + red Plexiglas 2444 provides a system for our purposes indistinguishable from the previous one, with no significant color term in the range $0.5 < B - R < 3$, as verified on our photometric material.

The plate material has been scanned with the COSMOS microdensitometer (MacGillivray & Stobie 1984) in IAM mode. The resulting tables, one per each plate, containing the instrumental magnitudes and other useful parameters for the objects detected, have been merged together in one table. Only objects with at least 3 detections in the 9 plates have been accepted in this final table containing 82 984 entries. The astrometric error box defining a common detection has been defined as a circle of 3.5 arcsec of radius. In this way spurious detections (plate defects) are minimized to an acceptable level, while real measurements are in practice never discarded.

of Cristiani and Vio (1990), and dereddened for galactic extinction according to Burstein and Heiles (1982).
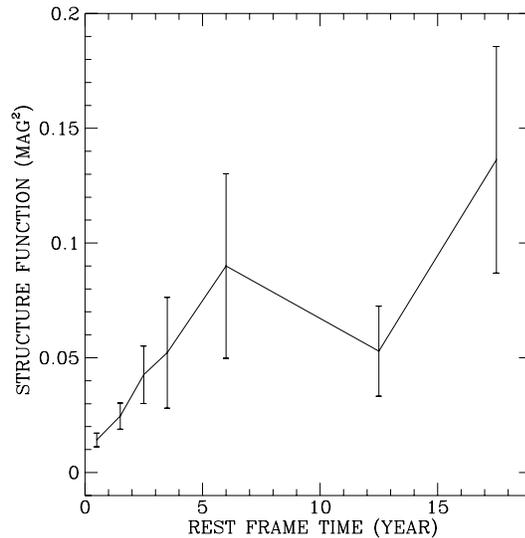
Fig. 1. QSO rest-frame structure function in the R-band

The calibration of the magnitudes of each plate has been carried out according to the following procedure (see also Paper I):

1. the magnitudes of 108 standard stars, transformed into the natural colour system of the plates, R', according to Eq. 1, have been used to derive for each plate a polynomial regression between instrumental and calibrated magnitudes.
2. the *median magnitude* of all the objects has been computed and each plate has been re-calibrated against the median magnitudes of the 27 111 point-like objects.
3. a procedure of uniformization of the usually spatially variable response of the photographic plates has been applied. Each plate has been subdivided in 10×10 sub-areas; for each of them the differences between the reference and the individual plate magnitudes have been computed and their distribution analysed. The zero-point shifts estimated in this way for each sub-area as a function of the magnitude have been smoothed and applied to the re-calibrated magnitudes. In the following we will refer to the magnitudes obtained in this way as R'_{final}.
4. for each plate the uncertainties of the R'_{final} magnitudes have been estimated by analysing the distribution of the differences $\Delta R = R'_{final} - R'_{median}$ as a function of the median magnitudes for all the point-like objects.
5. the completeness limit of each plate (see Table 2) has been estimated as the maximum of the histogram of the calibrated magnitudes.
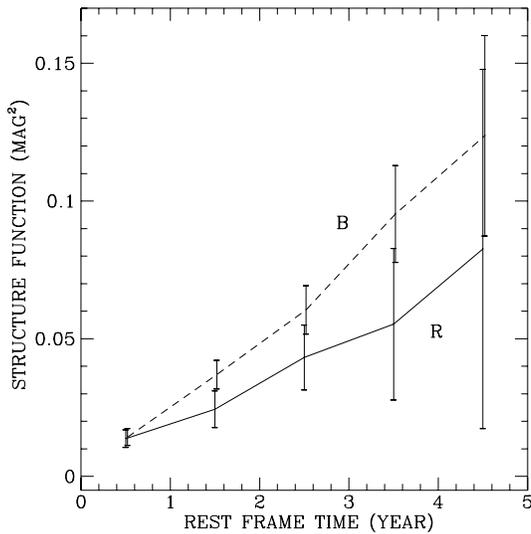
Fig. 2. Structure function for QSOs in the R-band (continuous line) and in the B-band (dashed line)

Fig. 3. ΔB_i vs. ΔR_i (see text). Dashed line: straight line with a slope 1. Continuous line: least-squares fit between ΔB_i and ΔR_i (see text). The cross in the lower-right corner shows the typical measurement errors

3. Statistical indices of the variability

3.1. The structure function

To study the ensemble variability properties of the SA94 sample we have used the structure function (Simonetti et al. 1985, Paper I), defined as:

$$SF(\tau) = \langle [\mathrm{mag}(t) - \mathrm{mag}(t+\tau)]^2 \rangle \qquad (2)$$

where $\mathrm{mag}(t)$ are the magnitudes at the time t, τ is a time lag evaluated in the rest-frame of each QSO and the brackets " $\langle \ldots \rangle$ " indicate a mean over the ensemble. The effect of the measurement errors has been subtracted according to the procedure described in detail in Paper I. Only objects detected in at least 5 epochs and with a median magnitude brighter than the completeness limit have been used to compute the SF. Only 6 QSOs have been measured on Plate R9477 brighter than the completeness limit. We have checked that the SF and the following statistical results do not depend on the inclusion/exclusion of these data.

In Fig. 1 the R-band SF in the quasar rest frame is shown. We observe a steady rise, steeper up to about 5 years and a flattening afterwards (within the errors), reaching values corresponding to about 0.1 mag^2 of RMS variability.

It should be noted that points in Fig. 1 with $\Delta t > 10$yr are all derived from the comparison of the POSS plate with the remaining plates. Being 28 years apart from Plate R5413, Plate E1453 does not play any role in the estimates of the SF on the shorter timescales (5 yr or less).

In Fig. 2 a comparison between the SFs in the B-band (as derived from the data discussed in Paper I) and in the R-band is reported. The SF in the B-band shows a larger variability amplitude with respect to the one in the R-band. To quantify the statistical difference between the two SFs, we have calculated the weighted average of the ratio $SF_{\mathrm{R}}/SF_{\mathrm{B}}$, for lags between
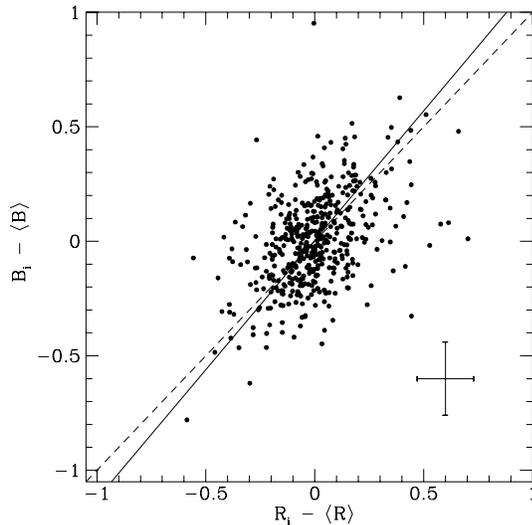
1 and 5 yr in the QSOs rest frame. The result is $SF_{\mathrm{R}}/SF_{\mathrm{B}} = 0.66 \pm 0.13$, a difference from the unity significant at a 2.5σ level.

In order avoid any possible bias deriving from different time samplings or time dilation effects, a direct comparison of the variability in the R and B band has been carried out. As shown in Fig. 3, for each object we have computed the quantities $\Delta R_i = R_i - \langle R \rangle$, as the difference between the magnitude at a given epoch and the average magnitude. Since the epochs of the R plates are in large part coincident with the epochs sampled with the B plates (epochs 2, 3, 4, 5, 6, 7 of the present paper correspond to epochs 2, 6, 8, 9, 10, 11+12 of Paper I, respectively) it has been possible to plot the ΔB_i versus the ΔR_i for all the objects with at least 5 epoch-magnitudes in common. Again, the POSS plate does not play any role in this comparison.

We have then fitted a straight-line relationship between ΔB_i and ΔR_i, with a least-squares technique that takes into account the errors of the data points on both axes (Fasano & Vio 1988). The result is $\Delta B = (1.130 \pm 0.054)\Delta R + (0.004 \pm 0.009)$. The dispersion of the points around this relation is fully compatible with the measurement errors, with no intrinsic scatter. If we make the additional assumption that the R flux varies in phase with the B flux, i.e. that for $\Delta R = 0$ $\Delta B = 0$, then we obtain $\Delta B = (1.130 \pm 0.054)\Delta R$, again fully consistent with no intrinsic scatter. The coefficient between the R and the B variability obtained in this way is consistent within the errors with what has been estimated on the basis of the SF analysis.

In Fig. 4 the distribution of QSOs in the redshift-magnitude plane is illustrated. To further investigate and disentangle the dependences of the variability on the luminosity and redshift we have examined two subsamples. The first is defined within the redshift limits $0.3 < z < 1.4$ (the area between the dashed lines in Fig. 4). The second is defined within the absolute mag-
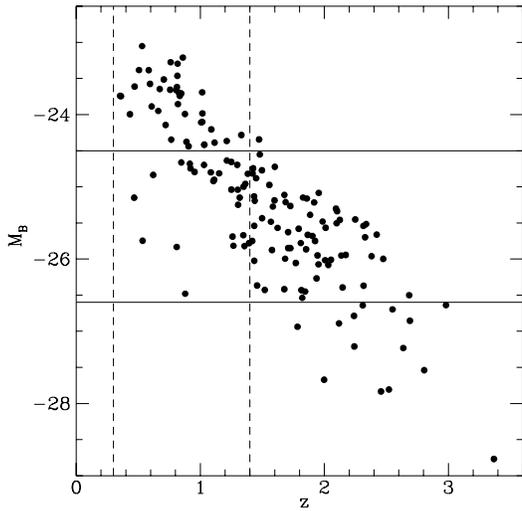
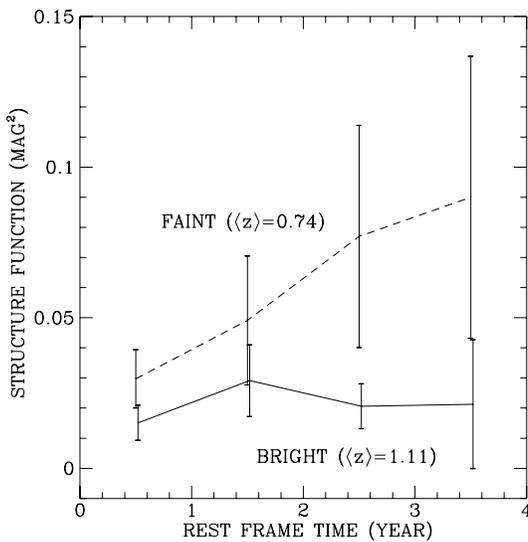**Fig. 4.** Distribution of the SA94 QSO sample in the $M_B - z$ plane

Fig. 5. The structure function for quasars of different luminosity in the redshift interval $0.3 < z < 1.4$. Continuous line: QSOs with $M_B \leq -24.5$. Dashed line: QSOs with $-24.5 < M_B$

Fig. 6. The structure function for quasars of different redshifts in the luminosity interval $-26.6 < M_B < -24.5$. Dashed line: QSOs with $z < 1.5$. Continuous line: QSOs with $1.5 \leq z$

Table 3. Correlation coefficients

	R	z	M_B
IDX	0.09 ± 0.08	-0.18 ± 0.08	0.24 ± 0.08
M_B	0.42 ± 0.07	-0.81 ± 0.03	$-$
z	0.15 ± 0.08	$-$	$-$

troduces a luminosity-redshift correlation in the data that may mask any redshift-variability correlation.

3.2. The variability index

In order to further verify the results obtained in the previous section, we have evaluated the variability index (IDX) for each QSO, defined as the variance of the normal process representing the intrinsic variability that, added to the photometric errors, reproduces the observed light variations on a given range of timescales (see Paper I). The index has been evaluated in one time bin (from 1 to 15 years in the QSOs rest frame) to avoid on the one hand time scales for which the structure function is still quickly rising, as observed in the previous section, and on the other hand time lags unaccessible with the present data for the higher-redshift QSOs. Then we have analysed the correlation matrix, reported in Table 3.

The correlation coefficients indicate a correlation of the variability index with the absolute magnitude and an almost equal anticorrelation with redshift (correlation coefficients respectively of +0.24 and −0.18, both with a significance greater than 99%). Due to the strong flux-redshift anticorrelation in the QSO sample it is not possible to disentangle if one of the two correlations is spurious. However, if, on the basis of the results of the previous subsections and of Paper I, we assume as fun-

nitude limits $-26.85 < M_B < -24.50$ (the area between the continuous lines in Fig. 4). As in Paper I, the SFs indicate that the QSO variability (in magnitude) is, also in the R band, clearly anticorrelated with absolute luminosity, in the sense that more luminous objects have a smaller variability amplitude (Fig. 5). No correlation between redshift and variability - of the type discovered in Paper I for the B-band variability - has been detected within the errors (Fig. 6). However, such a failure is not surprising considering that in the present work we are dealing with only one sample (in place of the three of Paper I) and the still non-uniform coverage of the redshift-absolute magnitude plane of the subsample defined between $-26.85 < M_B < -24.50$ in-
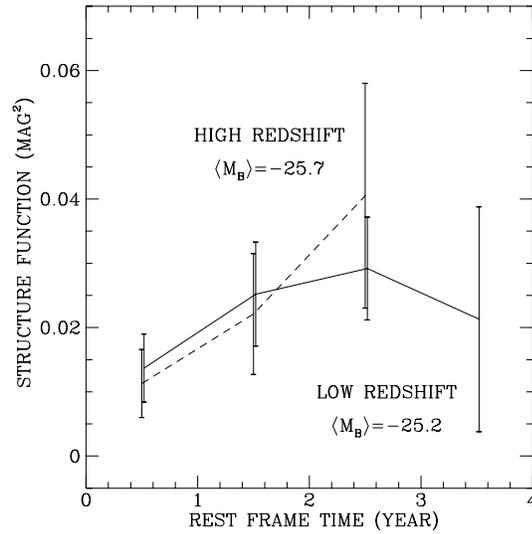
damental the absolute magnitude - variability correlation, it is possible to subtract its influence from the variability-redshift anticorrelation via the method of partial correlation analysis (Spiegel 1991). Applying this recipe to the results of Table 3, the corrected correlation coefficient between variability index and redshift, turns out to be 0.03 ± 0.08 (65%), not significant, in agreement with the result shown in Fig. 6.

4. Discussion

The decrease of the variability amplitude with increasing wavelength observed in the present QSO sample is consistent with the results obtained for individual objects at low redshift by Edelson et al. (1990), Kinney et al. (1991), Paltani & Courvoisier (1994). Is this variability-frequency correlation sufficient to account for the positive correlation between redshift and variability found in Paper I ?

Let us assume a simple power-law representation of a typical QSO spectrum (Giallongo et al. 1991, Di Clemente et al. 1996):

$$F_\lambda \propto \left(\frac{\lambda_0}{\lambda} \right)^\alpha \tag{3}$$

where F_λ is the flux at an observed wavelength λ, λ_0 an arbitrary wavelength and α the spectral index. The variability can then be modeled as a change in the spectral index:

$$F_\lambda(t) \propto \left(\frac{\lambda_0}{\lambda} \right)^{\alpha + \epsilon(t)} \tag{4}$$

where $\epsilon(t)$ is a function of time. In this way the flux variations are idealized as changes in the slope of the power-law "hinged" on the point of wavelength λ_0, that we imagine somewhere redwards of the B and R bands.
Converting in magnitudes,

$$M_R(t) = 2.5 \log \left[\frac{\lambda_R}{\lambda_0(1+z)} \right]^{\alpha + \epsilon(t)} + C, \tag{5}$$

we obtain the following expression for the magnitude variations:

$$\begin{aligned} \Delta M_R &= M_R(t_2) - M_R(t_1) = \\ &= 2.5[\epsilon(t_1) - \epsilon(t_2)] \log \left[\frac{\lambda_0(1+z)}{\lambda_R} \right] \end{aligned} \tag{6}$$

Applying the same equation to the B-band, we can write:

$$\frac{\Delta M_B}{\Delta M_R} = \frac{\log \frac{\lambda_0}{\lambda_B} + \log(1+z)}{\log \frac{\lambda_0}{\lambda_R} + \log(1+z)} \tag{7}$$

From Eq. 7 we would expect a decreasing ratio $\Delta M_B / \Delta M_R$ with increasing redshift. In the present data we observe, if any, a very small decrement of $\Delta M_B / \Delta M_R$ with the redshift (from 1.14 ± 0.08 to 1.10 ± 0.09 for two sub-samples with redshift $z < 1$ and $1 < z \le 1.8$ respectively).

Introducing the value of $\Delta M_B / \Delta M_R = 1.13 \pm 0.05$ at a $\langle z \rangle \sim 1.5$ reported in Sect. 3 in Eq. 7, allows us to put a lower limit to the wavelength $\lambda_0 \gtrsim 31\,000$ Å.

If we turn back to Eq. 6, we can see how this lower limit to λ_0, together with the typical observed RMS for the variability ΔM_B and ΔM_R of 0.35 and 0.28 mag, respectively (see Fig. 2), puts an upper limit to the RMS variation of the spectral index $\sigma_\epsilon \lesssim 0.11$.

This value can be compared with the typical dispersion in the spectral indices observed in various QSO samples: Pei et al. (1991) have obtained $\sigma_\alpha \sim 0.24$ in a control sample of 15 QSOs, Francis (1993) observed $\sigma_\alpha \sim 0.5$ in a much larger sample, showing also a systematic hardening of the spectrum with increasing redshift. In this way the dispersion in the observed spectral indices of the QSO population can be only partially accounted for by variability and significant intrinsic differences between QSO and QSO have to be invoked (but see also the dispersion $\sigma_{\alpha_{ox}} \sim 0.1$ estimated by Elvis et al., 1994).

Putting in Eq. 6 our best estimates for $\sigma_\epsilon = 0.07$ and $\lambda_0 = 86\,000$ Å, we obtain for the typical RMS variability in the B band 0.26 and 0.33 mag at $z = 0.5$ and $z = 3$, respectively and 0.22 and 0.30 in the R band at the same redshifts, consistent with the observations of Paper I.

The dependence of the variability time scale on the wavelength is a standard prediction of the accretion disk model. The temperature of the disk decreases with the radius, and the dynamical, thermal and viscous time scales all increase as $r^{3/2}$ (see Baganoff & Malkan 1995 and references therein). In particular, in the standard model, involving instabilities in a thin accretion disk around a supermassive black hole, the intrinsic characteristic time scale should vary as $\tau \propto \lambda^2$. More in general, if the source is thermal and if the flux variability is due to temperature changes, the observed wavelength dependence can be naturally produced (Paltani & Courvoisier 1994). The only requirement concerns the turnover in the spectral energy distribution that should not be located at such a high frequency that the spectral slope in the observed band becomes independent of the temperature (e.g. the Rayleigh-Jeans domain for a black body spectrum). As remarked by Di Clemente et al. (1996), if brighter objects are on average hotter and the variability is due to temperature changes, one would expect a negative correlation between amplitude of the variability and luminosity, as observed. Assuming for example a spectrum of black body or thermal bremsstrahlung, the spectral turnover of brighter objects is progressively shifted at higher frequencies producing progressively smaller flux changes, from $\delta I/I \propto \delta T/T(h\nu/kT)$ for $kT < h\nu$, to $\delta I/I \propto \delta T/T$ for $kT > h\nu$.

The broad-band variability in the starburst model (Aretxaga et al. 1996 and references therein) is defined by the superposition of a variable component, supernova explosions (SNe) generating rapidly evolving compact supernova remnants (cSNR), and a non-variable component, a young stellar cluster and the other stars of the galaxy. The problem of predicting the wavelength dependence of the variability can be reduced to computing the spectra of the variable and non-variable components, and their relative luminosities. The spectrum of the

non-variable component has been predicted to show a $F_\nu \propto \nu^\alpha$ with $\alpha \sim -1.0 \div 0$ (Cid Fernandes & Terlevich 1995). The variable/non-variable relative luminosities can also be estimated on the basis of stellar evolution (Aretxaga & Terlevich 1994). Much more difficult is to predict the optical/UV spectrum of the variable component. It is expected to be harder than the non-variable component with a $F_\nu \propto \nu^\alpha$ and $\alpha \sim 0.5$. We can model the total QSO flux according to a Simple Poissonian model (Cid Fernandes et al. 1996) as

$$F_\text{tot} = F_\text{var} + F_\text{bck} =$$
$$= (1 - f_\text{bck}) \left(\frac{\lambda}{\lambda_0}\right)^{(\alpha_\text{var}-2)} + f_\text{bck} \left(\frac{\lambda}{\lambda_0}\right)^{(\alpha_\text{bck}-2)} \quad (8)$$

where f_bck is the non-variable fraction of the total flux and α_bck, α_var are the slopes of the non-variable and variable components. Indicating with λ_B and λ_R the effective wavelengths of the B and R-band and putting for simplicity $\lambda_0 = \lambda_\text{B}$, we obtain for the ratio between the B-band and R-band variability:

$$\frac{\Delta M_\text{B}}{\Delta M_\text{R}} = \frac{f_\text{bck} \left(\frac{\lambda_\text{R}}{\lambda_\text{B}}\right)^{\Delta\alpha} + f_\text{var}(1+z)^{\Delta\alpha}}{f_\text{bck} + f_\text{var}(1+z)^{\Delta\alpha}} \quad (9)$$

with $\Delta\alpha = \alpha_\text{bck} - \alpha_\text{var}$.

For example, with $\Delta\alpha = 1$ and $f_\text{bck}, f_\text{var} = 0.7, 0.3$ respectively (Cid Fernandes et al. 1996), the ratio between the B-band and R-band variability is expected to be about 1.4 at $z = 0$, tending to 1 for increasing redshift, independent on the intrinsic luminosity of the QSO. The above reported slight tendency for a decreasing $\Delta M_\text{B}/\Delta M_\text{R}$ ratio with increasing redshift is compatible with this model. However, an increase of the $\Delta M_\text{B}/\Delta M_\text{R}$ with the absolute luminosity is also observed. We find the values $\Delta M_\text{B}/\Delta M_\text{R} = 1.08 \pm 0.06$ and $\Delta M_\text{B}/\Delta M_\text{R} = 1.31 \pm 0.11$ for two subsamples with $M_\text{B} > -25.2$ ($\langle z \rangle = 1.05$) and $M_\text{B} < -25.2$ ($\langle z \rangle = 1.92$), respectively. This suggests that more general situations have to be envisaged in which the fraction on the non-variable component and/or the pulse properties (e.g. the spectral distribution) depend on the global luminosity of the object.

Recently Hawkins (1996) has proposed that the variability of nearly all the QSOs (except the very low redshift ones) is produced by microlensing. A non-achromatic behaviour can be accommodated in this kind of model. For a source comparable in size to the Einstein ring of the lens, with a quasar disk redder at larger radii, the bluer compact core would produce a larger amplitude of the variations in the blue passband whereas the larger extent of the red image would cause a small amplitude variation, albeit with a longer duration, in the red. However it cannot be denied that achromatic light variations would have been one of the most significant characteristics of the microlensing model and the present observation of the wavelength dependence make it less appealing/compelling. In particular the superposition of the two competing effects of time dilation and correlation of the variability with frequency, i.e. redshift, accounts naturally, also in the accretion disk and in the starburst scenarios, for the observed lack of correlation in the observer's rest frame between

the variability time scale and the redshift, otherwise claimed as an evidence in favor of the microlensing model.

Future detailed comparisons between simulated and observed light curves will be fundamental to disentangle among these three scenarios and to start exploring the parameter space of each model.

References

Aretxaga I., Terlevich R., 1994, MNRAS 269, 462

Aretxaga I., Cid Fernandes R., Terlevich R., 1996, MNRAS submitted

Barbieri C., Cristiani S., 1986, A&AS 63, 1

Baganoff F.K., Malkan M.A., 1995, ApJ 444, L13

Bessel M.S., 1986, PASP 98, 1303

Cid Fernandes R., Terlevich R., 1995, MNRAS 272, 423

Cid Fernandes R., Aretxaga I., Terlevich R., 1996, MNRAS submitted

Cristiani S., Vio R., 1990, A&A 227, 385

Cristiani S., La Franca F., Barbieri C., Clowes R.G., Iovino A., 1991, MNRAS 250, 531

Cristiani S., Trentini S., La Franca F. et al., 1996, A&A 306, 395

Di Clemente A., Giallongo E., Natali G., Trevese D., Vagnetti F., 1996, ApJ 463, 466

Edelson R., Krolik J., Pike G., 1990, ApJ 359, 86

Elvis M., Wilkes B.J., McDowell J.C. et al., 1994, ApJS 95, 1

Fasano G., Vio R., 1988, 'Newsletter of the Working Group for Modern Astronomical Methodology' 7, 2

Francis P.J., 1993, ApJ 407, 519

Giallongo E., Trevese D., Vagnetti F., 1991, ApJ 377, 345

Hawkins M.R.S., 1993, Nature 366, 242

Hawkins M.R.S., 1996, MNRAS 278, 787

Hook I.M., MacMahon M.G., Boyle B.J., Irwin M.J., 1994, MNRAS 268, 305

Kinney A.L., Bohlin R.C., Blades J.C., York D.G., 1991, ApJS 75, 645

La Franca F., Cristiani S., Barbieri C., 1992, AJ 103, 1062

Mac Gillivray H.T., Stobie R.S., 1984, Vistas in Astronomy 27, 433

Paltani S., Courvoisier T.J.-L., 1994, A&A 291, 74

Pei Y.C., Fall S.M., Bechtold J., 1991, ApJ 378, 6

Perola G.C. et al., 1982, MNRAS 200, 293

Rees M., 1984, ARAA 22, 471

Simonetti J.H., Cordes J.M., Heeschen D.S., 1985, ApJ 296, 46

Spiegel M.R., 1991, Schaum's outline of Theory and problems of Statistics, 2nd ed, McGraw-Hill, Inc., pag. 327

Terlevich R., Tenorio-Tagle G., Franco J., Melnick J., 1992, MNRAS 255, 713

Trevese D., Kron R.G., Majewski S.R., Bershady M.A., Koo D.C., 1994, ApJ 433, 494

Véron P., Hawkins M.R.S., 1995, A&A 296, 665

Véron-Cetty M.P., Véron P., 1993, *A Catalogue of QSOs and Active Galactic Nuclei (6th Edition)*, ESO Scientific Report, N. 13

Warren S.J., Hewett P.C., Irwin M.J., Osmer P.S., 1991, ApJS 76, 1